DOI 10.24425/aee.2024.149920

Active parallel compensation using a power supply with a tunable inductive filter

ŁUKASZ CIEPLIŃSKI✉, **ADAM GULCZYŃSKI**

Poznan University of Technology, Faculty of Control, Robotics and Electrical Engineering
Piotrowo 3A, 60-965 Poznan, Poland

e-mail: ✉ *Lukasz.cieplinski@put.poznan.pl*

(Received: 22.08.2023, revised: 17.04.2024)

Abstract: Increasing numbers of devices of various types are now connected to power lines. Their nonlinear nature harms the operation of the lines, as the line voltage is distorted from a sine wave, which causes disturbances in the operation of other loads. This study proposes a method of active parallel compensation that can be realised using a power supply. The proposed device is a dual-function system: it supplies the load connected to its DC link, and operates as a parallel active filter. This kind of device, with a relatively low value of the rated output power, could be implemented in electrical systems to provide distributed compensation. The second novel aspect of this work is the use of a tunable inductive filter, which is included at the input of the power electronics controlled current source and forms a main part of the power supply. The use of this tunable inductive filter increases the frequency response of the current source, while at the same time, in the quasi-steady state of power supply operation, the pulse modulation component of the input current source remains at a minimum level. This paper discusses the structure of an electrical system with the proposed power supply and the rules of operation for the system, and presents test results based on both a simulation and a laboratory model of the system.

Key words: Power Factor Correction, Power Quality, Power Supply, Reactive Power, Shunt Active Power Filters

1. Introduction

1.1. Impact of converter systems on the operation of the power grid

The main reasons for the unfavourable impact of converter systems on the operation of the power grid are their nonlinearity, non-stationarity and the generation of voltage and current transients, which occur in the dynamic states of operation of both these systems and the power

line [1, 2]. Conventional solutions based on diode and thyristor circuits cause unfavourable effects on the power line, such as voltage commutation notches and distortion of the current waveform from a sinusoidal shape [3–5].

1.2. Methods of reducing the adverse effects of nonlinear loads on the power grid

Most modern devices are designed such that their power factor approaches unity, i.e. they are equipped with a Power Factor Correction (PFC) function [6, 7]. However, control is only exerted over their input current. This requires minimising the reactive power input from the power grid and reducing the distortion of the grid current (minimising the value of its higher harmonics). Historically, the oldest devices that have been used to minimise the impact of a nonlinear load on the grid operation are passive power filters [8, 9]; however, these filters allow for only a limited reduction in reactive power, since their characteristics are determined in the filter at the design stage. Thus, Shunt Active Power Filters (SAPF) are often necessary [10–12], although due to their high cost [13], hybrid filters are also used [14, 15].

1.3. Indicators for assessing the impact of loads on the operation of the network

The quality of power is considered acceptable if the deviation between its values and the rated ones is within a level imposed by the relevant electric power authorities [16]. However, it should be noted that with regard to deformed waveforms, there is no consensus among researchers on how to define energy indicators [17–20].

The following parameters have been used to determine the quality of energy:

– *TWD* – the total waveform distortion [21]:

$$TWD = \frac{\sqrt{I_{\mathrm{RMS}}^2 - I_{1,\mathrm{RMS}}^2}}{I_{1,\mathrm{RMS}}} = \sqrt{\frac{I_{\mathrm{RMS}}^2}{I_{1,\mathrm{RMS}}^2} - 1}, \tag{1}$$

– $\cos\varphi_{\mathrm{L}}$ is a power factor according to the Budeanu power theory [18]. In the case of monoharmonic waveforms,

$$\cos\varphi_{\mathrm{L}} = \frac{P_{\mathrm{L}}}{S_{\mathrm{L}}}, \tag{2}$$

– τ_{L} is the duration of a specific transient state in the power supply input current.

The rationale for using the *TWD* coefficient in this paper, rather than evaluating the distortion of the signal from a sinusoidal waveform, is related to the almost permanent dynamic state of the real power grid [2].

2. Active parallel compensation of distorted current

2.1. Structure of the power supply compensator with tunable inductive filter

A block diagram of an electrical system with a power supply compensator, cooperating with a group of nonlinear loads connected to the same grid node as the power supply (PSP), is shown in Fig. 1.

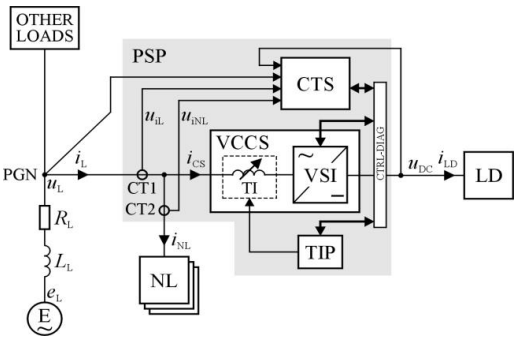

Fig. 1. Block diagram of an electrical system with a power supply, equipped with both an active parallel compensation function and a tunable inductive filter

The tunable inductive filter (TI) at the input of the voltage inverter (VSI) is characterised by variable inductance, the value of which is controlled by the dedicated power block (TIP), which, in turn, is under the control of the power supply control section (CTS).

The power theory developed by Fryze [17] was chosen to control the compensation function of the PSP. The general goal of optimising the network current (i_{L}) is to minimise its RMS value. The controlled current source (VCCS block) forces a suitably distorted current to flow at its input, which, when combined with the current of the nonlinear load, will give a resultant current with a (theoretically) sinusoidal shape:

$$i_{\mathrm{L}}(t) = i_{\mathrm{NL}}(t) + i_{\mathrm{CS}}(t) = i_{\mathrm{ref,L}}(t) = I_{\mathrm{ref,I}} \sin(\omega_{\mathrm{L}} t), \tag{3}$$

where $I_{\mathrm{ref,I}}$ is the amplitude of the reference current.

2.2. Influence of the power block on the dynamic parameters values of the power supply

The input power stage of the power supply is an H-type transistor bridge with an inductive filter (L_{CS}) at the input, as shown in Fig. 2. This circuit forms a power electronic controlled current source (VCCS) [22]. Its tasks are to provide the required voltage (u_{DC}) in the DC link of the power supply and to actively compensate for the phase shift and higher harmonics of the nonlinear load (NL block) current.

The VCCS current waveform (i_{CS}) is described by the following formula, which does not take into account the resistance of the filter, the impedance of the grid or the voltage drops across the transistors in the converter:

$$i_{\mathrm{CS}}(t) = \frac{1}{L_{\mathrm{CS}}} \int [u_{\mathrm{DC}}(t) - |u_{\mathrm{L}}(t)|]\, \mathrm{d}t. \tag{4}$$

The ability of a current source to shape the input current is mainly determined by the value of its bandwidth (BW), or the frequency response in relation to its linear model [22]:

$$BW = \frac{1}{2\pi I_{\mathrm{CS}}} SR, \tag{5}$$

where I_{CS} is the maximum amplitude of the controlled current source, and SR is the limiting value of the rate of change of the source output current (specified in A/s).

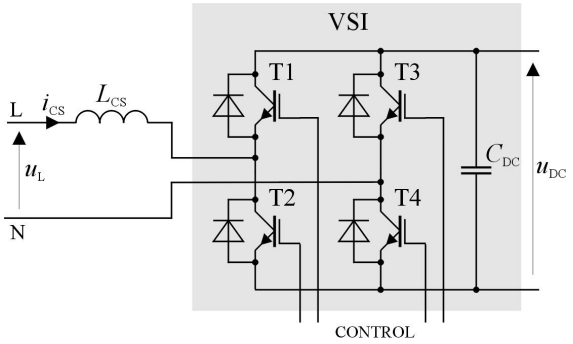

Fig. 2. Schematic diagram showing the input power stage of the PSP associated with the power electronic controlled current source

Referring only to the first half-period of the grid voltage, *SR* reaches two extreme values:

$$SR_{\max} = \frac{1}{L_{CS}} u_{DC}(t_0)\,|t_0 = 0\,, \tag{6}$$

$$SR_{\min} = \frac{1}{L_{CS}} \left[u_{DC}(t_1) - U_L\right]\Big|t_1 = \frac{\pi}{2\omega_L}\,, \tag{7}$$

where U_L is the amplitude of the voltage at the grid node.

Hence, if we assume that the values of both the line voltage and the DC voltage are set in advance, the dynamics of the changes in the VCCS input current can be increased only by reducing the value of the filter inductance. However, this would result in an increase in the value of the carrier component of pulse-width modulation (PWM). Thus, in order to extend the frequency response of the PSP, a tunable inductive filter was used.

3. Principle of operation of the proposed tunable inductive filter

To create a tunable inductive filter, the phenomenon of coupling between the magnetic fluxes of two coils was exploited (Fig. 3). Their resultant magnetic fluxes can be strengthened or weakened, which causes a change in the overall inductance. The value of the equivalent impedance (Z_{TI}) of the filter can reach two values. The equation below is used for the value of the equivalent reactance of the filter, which depends on the coupling coefficient k and the state of the key S:

$$X_{TI} = \left(1 - s_{T-TI}k^2\right) X_1\Big|_{S_{T-TI}=0 \,\vee\, S_{T-TI}=1}\,, \tag{8}$$

where $s_{T-TI} = 0$ represents the key-open state, and $s_{T-TI} = 1$ represents the key-closed state.

The main role in this circuit is played by a transformer with a magnetic flux coupling coefficient of $k = 0.85$.

The transmittance of the small-signal model of the developed passive filter is as follows:

$$Z(s) = sL. \tag{9}$$

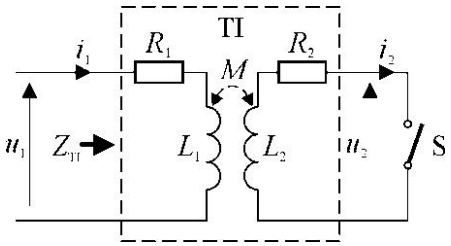

Fig. 3. Diagram showing the principle of operation of the proposed tunable inductive filter

Thus far, changes in inductance have been created by combining inductances and reconfiguring individual chokes, or by more advanced methods involving core magnetisation [23–26], which have lower energy efficiency (than proposed solution in this work) due to DC-bias current conditioning.

Since this study is a continuation of the author's previous work. More information on the proposed tunable inductive filter can be found in [27–29].

4. Power supply control section

A block diagram of the power supply control section (CTS) is shown in Fig. 4. The functionality of each block has been described in detail in previous work [27], and only a brief summary of the structure of the system is given here for the reader's convenience.

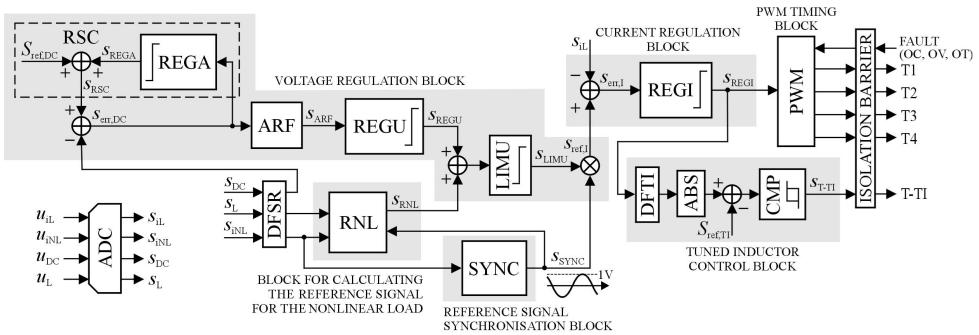

Fig. 4. Block diagram showing the power supply compensator control system

The control system consists of the following main blocks:

– The voltage regulator block, which is responsible for ensuring the correct value of the voltage in the DC link of the power supply.
– The block for calculating the reference signal for the nonlinear load (RNL), which computes the value of the reference signal for the current regulator in relation to current active power of the nonlinear load. The operation of this block is based on Fryze's power theory.
– The reference signal synchronisation block (SYNC), which generates a unity-amplitude sine-wave signal that is phase-synchronised with the voltage in the power line node.
– The current regulation block, which is responsible for the generation of a suitable VCCS input current (in terms of its shape).
– The tuned inductor control block, which generates the control signal for the TIP block.

5. Simulation model of the power supply

5.1. Structure and parameters of the model

Simulation studies were carried out in the ORCAD/PSpice environment, using suitably modified component models provided in libraries, in order to best replicate the performance characteristics of the components used in the laboratory model of the power supply.

The individual blocks of the control system in the simulation model were also realised in digital form, using elements of the ORCAD environment libraries, similarly to those used for the physical realisation of the controllers and similar blocks, i.e. IIR or FIR filter structures. These elements consisted of sampling and memory blocks, signal adders, and multiplier circuits. In contrast, the structurally complex RNL and SYNC blocks were modelled in a simplified form in the simulation, using signal sources with predetermined parameter values. The DFSR block (the decimation filter) was not included in the simulation model; instead, two values of the signal sampling frequency were used (denoted as $f_{s,1}$ and $f_{s,2}$). This arrangement was directly related to the structure of the control algorithm for the physical model of the power supply. It should be noted that the high value of the frequency ($f_{s,2}$), based on which the current control block and the tunable filter control block operated, resulted from the requirement for effective shaping of the controlled source current in the transient state by the TIC and TIP blocks. This value was selected based on tests of the power supply simulation model, and gave rise to a need for significant computing power for the digital control system of the experimental model of the power supply.

Simulation and laboratory models' parameters were consistent and are presented in Table 1.

Table 1. Parameters of the electrical system with the PSP

No.	Parameter	Symbol	Value
No.	**Parameter**	**Symbol**	**Value**
Power grid and power supply ratings			
1	RMS grid voltage	$U_{L,RMS}$	230 V
2	Power grid voltage frequency	f_L	50 Hz
3	Power grid resistance	R_L	0.5 Ω
4	Power grid inductance	L_L	0.4 mH
5	Rated output power of the PSP	$P_{DC,nom}$	1.2 kW
6	DC voltage and its setting range	$U_{DC,n}$	375 ± 25 V
Parameters of the VCCS			
8	Inductance of TI: S-switch open	L_{TI}	4.52 mH
9	Inductance of TI: S-switch closed	L_{TI}	1.51 mH
10	Capacitor in the DC link	C_{DC}	1 mF
11	PWM carrier frequency	f_c	10 Hz

5.2. Simulation studies

In the simulation model, a thyristor voltage regulator, loaded by a resistor (T-R type load), was used as a nonlinear load. The power of the NL block was set to 50% of the nominal output power of the power supply relative to the DC link. The firing angle of the individual thyristor was set to 90 el. deg.

Figure 5 shows some example results of model tests with respect to the power supply current and NL block current, for inductive filters with fixed (Fig. 5(a)) and variable inductance (Fig. 5(b)) and with the compensation function enabled. The waveforms shown here represent operation of the model with the rated voltage in the DC link and the rated load power in this link. Differences can be seen in both the current waveform of the power supply and the current in the NL block, and the performance of the variant of the power supply with a tunable filter is superior. In this case, the duration of the transient, in the form of a current peak, is reduced to about 40% of that of the variant of the system with a fixed inductance filter.

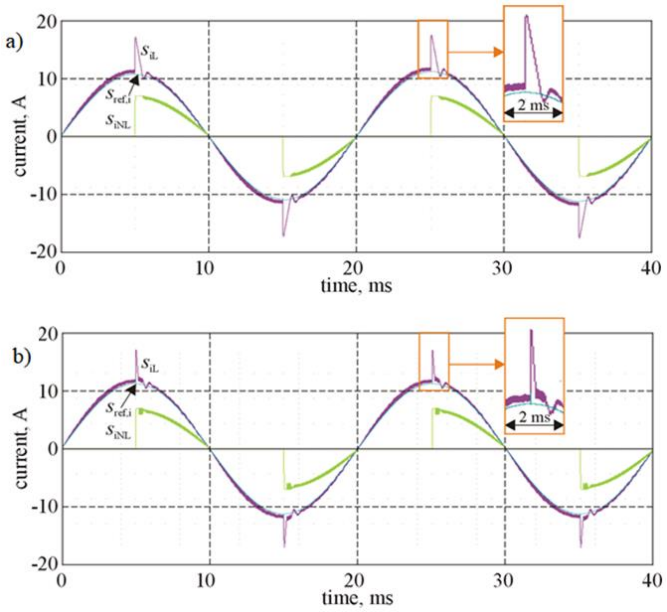

Fig. 5. Waveforms of the reference signal, the resultant current of the power supply, the current of the NL block and the current of the nonlinear load itself, with the compensation function enabled and the use of (a) a fixed and (b) a tunable inductive filter

Figure 6 shows the output signal of the current regulator (S_{REGI}) and the signal controlling the power part of the tunable inductive filter ($S_{\mathrm{T-TI}}$), under the rated operating conditions of the power supply. Based on the operation principle of the control system, the input of the current regulator in the saturation state initiates the operation of the tunable filter control block (TIC).

Comparative tests were also performed on the value of the control error signal for the current regulator (REGI), for both types of inductive filters. The behaviour of this signal under the rated operating conditions of the system simulation model is shown in Fig. 7.

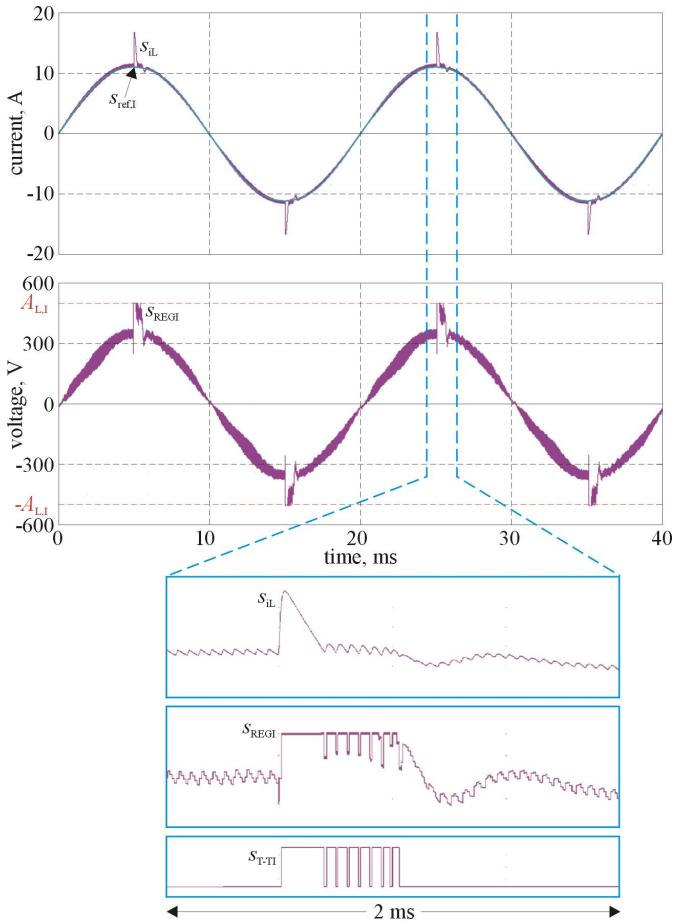

Fig. 6. The waveforms related to the interaction of tunable filter control block with the current regulator

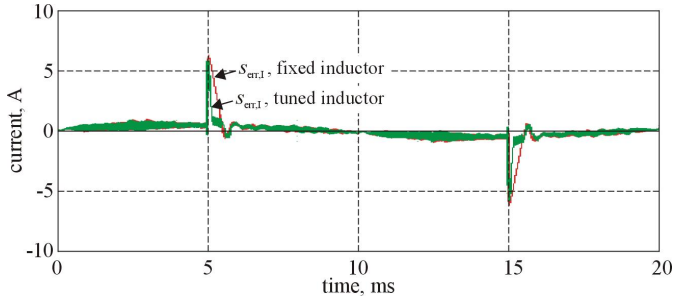

Fig. 7. Waveforms of the error signal in the current control block for tuned and fixed inductor

These waveforms are almost identical except for the transient state at the output of the current regulator, which is related to its saturation. In order to quantitatively assess the quality of the control, a formula was used to define the value of the control error [30] ($\varepsilon_{\mathrm{REGI}}$) as a relation

between the RMS value of the control error signal ($S_{\mathrm{err,I,RMS}}$) and the reference signal for the current regulator ($s_{\mathrm{ref,I}}$), i.e. a sine wave:

$$\varepsilon_{\mathrm{REGI}} = \sqrt{2}\frac{S_{\mathrm{err,I,RMS}}}{S_{\mathrm{ref,I}}}100\%, \tag{10}$$

where $S_{\mathrm{ref,I}}$ is the amplitude of the reference signal.

The value of the $\varepsilon_{\mathrm{REGI}}$ parameter was 12.2% for the simulation model with a constant inductance filter, and 9.0% for the model with a variable inductance filter.

Figure 8 shows the relationship between the *TWD* coefficient and the transient state τ_{L} of the resultant current and the voltage on the DC link, for a power supply output power equal to the nominal value. The results indicate about decrease by a factor of 1.5 in the value of the *TWD* parameter, and a reduction by a factor of about 2.4 in the duration of the transient state in the case of a power supply with a tunable inductive filter, compared to the traditional solution. Figure 8 confirms the correctness of Formulas 5, 6 and 7. For lower voltages on the DC bus, the advantage of using a tunable induction filter is greater.

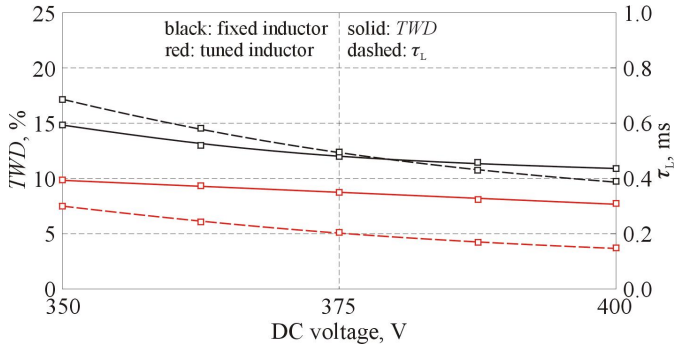

Fig. 8. *TWD* and τ_{L} plots of the input current for the PSP simulation model vs. DC link voltage

Figure 9 shows the spectrum of the PSP input current.

The last test of the simulation model was carried out to assess the static and dynamic errors in the voltage regulation on the DC link, relative to the operation of the voltage regulation block, in response to a step change in the load value on the DC link.

In the upper part of Fig. 10, the s_{REGU} parameter can be seen to assume a constant value in the steady state of operation. This proves the correctness of the operational concept of the anti-ripple filter (ARF) block in terms of eliminating from the input signal of the voltage regulator (REGU) the ripple component associated with the voltage waveform on the DC link.

In the steady state of operation of the system, the average value of the DC voltage on the DC link was very close to the reference voltage value for the voltage regulator, thanks to the operation of the RSC unit. The average value of the error was about 1 V, i.e. about 0.27% of the preset signal value. The value of this error is independent of both the voltage set on the DC link and the load value. The duration of the dynamic state of the voltage on the DC link, after a step change in its load (calculated up to the point where 90% of the set value of this voltage was reached), was equal to about two periods of the mains voltage.

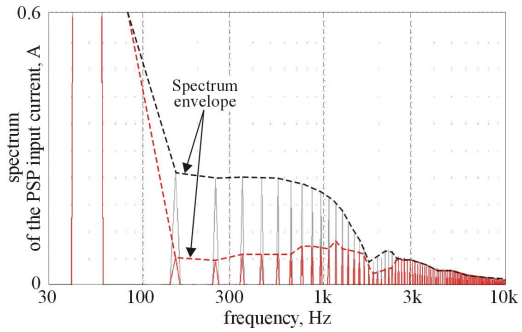

Fig. 9. Current spectrum for the electrical system (fixed inductance shown in grey; variable inductance shown in red), The amplitude of the fundamental harmonic current was approximately 11.1 A

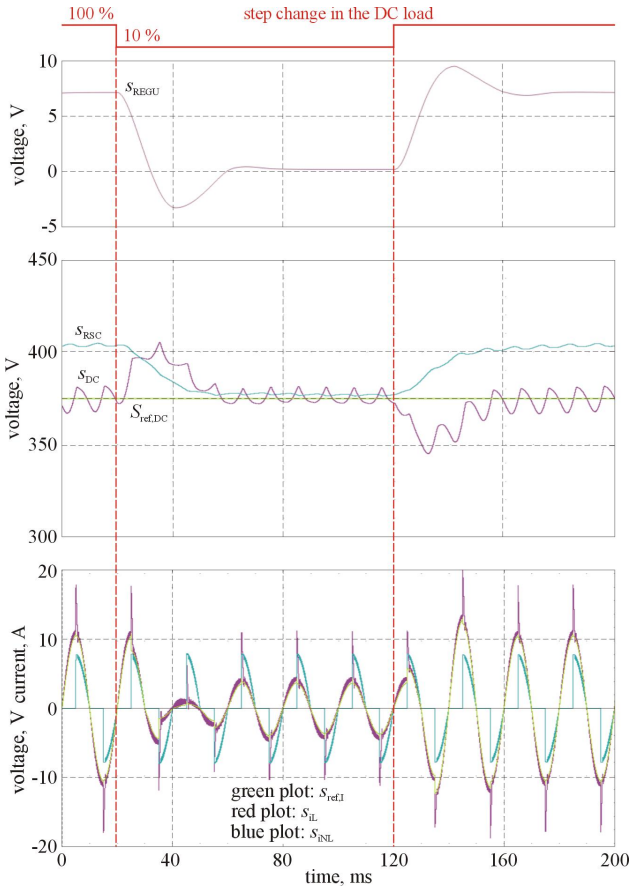

Fig. 10. Characteristic waveforms for the simulation model showing the response of the power supply to a step change in the value of the DC link load

6. Laboratory model of the power supply

6.1. Laboratory setup

In the power stage of the laboratory model of the PSP, a laboratory inverter of type P3-5-550MFE LABINVERTER [31] was used. An evaluation system of type ALS-G3-1369 [31] was used in the control section of the PSP. A general view of the laboratory setup is shown in Fig. 11.

The power supply control algorithm was consistent with its block diagram, as shown in Fig. 4. The full versions of all blocks of the control system for the power part of the power supply were implemented in the model, using the operational algorithms described in [27].

The values of some parameters of the model were corrected in relation to the assumptions made in the simulation model, due to the real conditions of operation. These corrections were made to the following blocks: the decimation filter (i.e. the DFSR block, which was included in the laboratory model), the full implementation of the SYNC and RNL blocks, and the filter control induction.

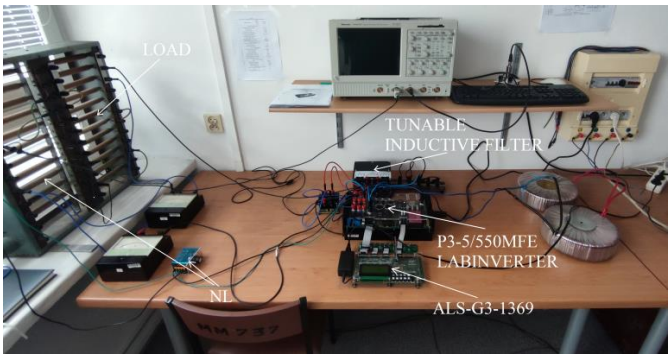

Fig. 11. General view of the laboratory setup

The signals were recorded and visualised, and an analysis of their parameters was carried out using a four-channel TDS3054B digital oscilloscope (TEKTRONIX) and the PLOT function of the VisualDSP++ environment. The measured bandwidth for the oscilloscope was found to be 31.125 kHz.

6.2. Power supply tests for T-R load type

The results from the model tests were divided into two groups. The first sets were related to the assessment of the parameter values TWD, τ_{L} and $\varepsilon_{\mathrm{REGI}}$, while the second sets were related to the quality of voltage regulation in the DC link, in terms of the value of the static error and the response time of the system to a step change in the load value.

Figure 12 shows exemplary waveforms for the nonlinear load current, the reference signal for the current regulator, and the input current of the power supply. These were recorded for a nonlinear load power equal to 50% of the nominal power of the power supply on the DC side of the PSP.

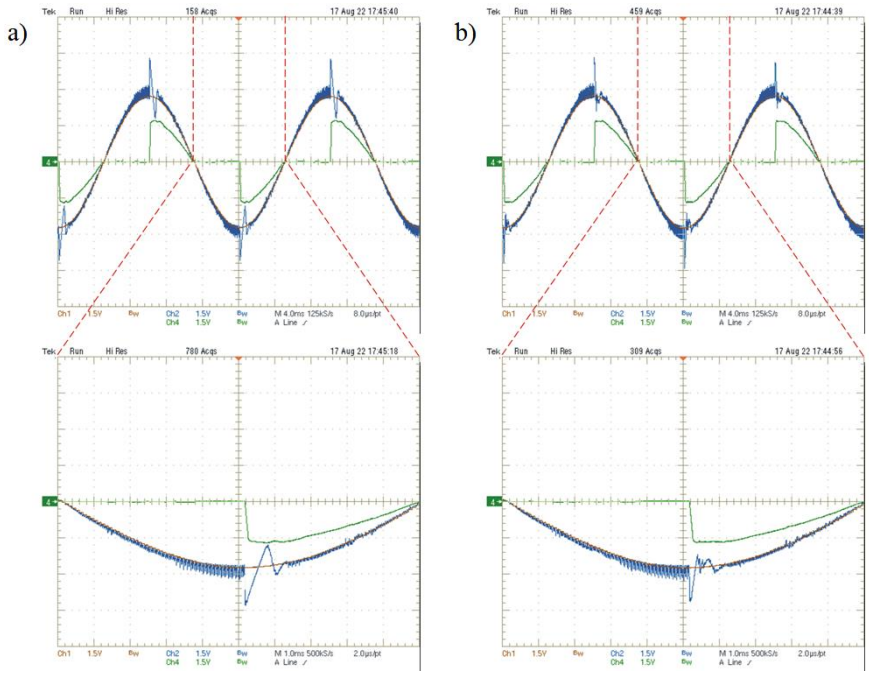

Fig. 12. Waveforms for the laboratory model for the nominal power and voltage on the DC link: (a) L_{TI} = const; (b) L_{TI} = var (red: reference signal for current regulator; blue: PSP input current; green: NL block current; vertical axis scale: 6 A/div)

Based on the recorded data, the values of the control error were determined ($\varepsilon_{\mathrm{REGI}}$). At the nominal value of the output power, these were 14.0% and 9.3% for constant and variable values of the inductive filter, respectively.

Curves for the *TWD* coefficient of the PSP input current and the transient state τ_{L} in this current were plotted versus the voltage in the DC link, as shown in Fig. 13. This figure is functional equivalent of Fig. 8.

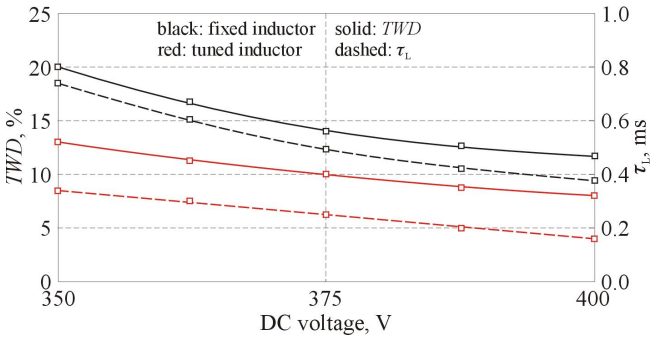

Fig. 13. *TWD* and τ_{L} plots of the input current in the PSP laboratory model vs. the DC link voltage

Figure 14(a) shows the waveforms in the system in the case where the load was disconnected from the DC link; functionally, the tested system became a typical active parallel filter (except for the newly introduced function of the tunable inductive filter). Figure 14(b) shows the waveforms in the system in the case where the nonlinear load was disconnected from the network; functionally, the circuit became a power supply equipped with a PFC function.

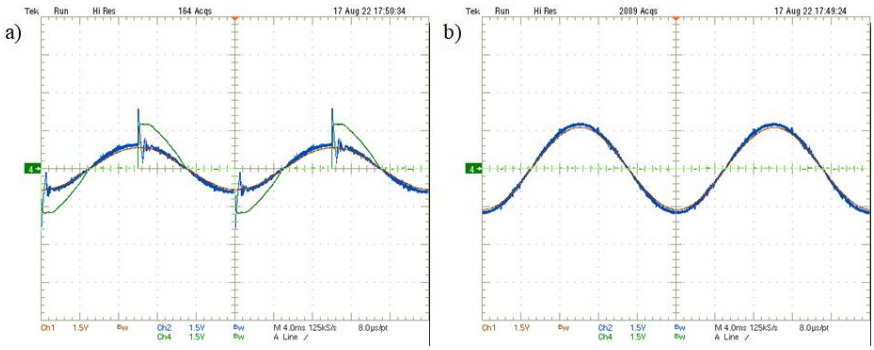

Fig. 14. Waveforms for the laboratory model of the PSP for variable L_{TI} and for: (a) the load disconnected from the DC link; (b) the nonlinear load disconnected from the system (red: reference signal for current regulator; blue: PSP input current; green; NL block current; vertical axis scale: 6 A/div)

Figure 15 shows the details of the signal waveforms in the inductive filter control system in their transient state in connection with the activation of the TIC block. This plot is functional equivalent of Fig. 6.

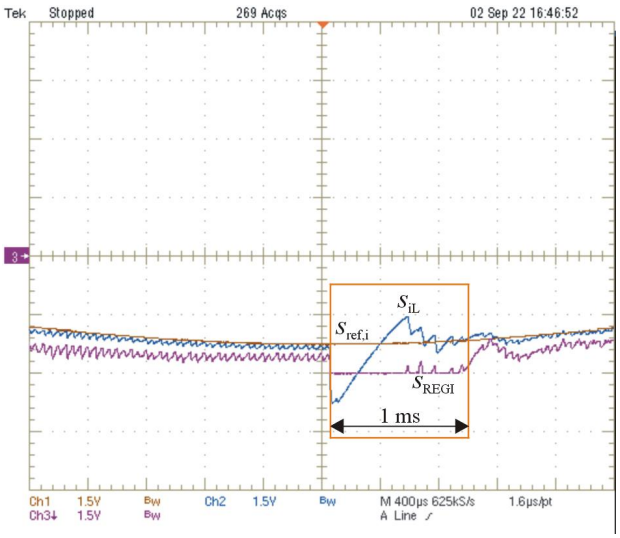

Fig. 15. Details of the waveforms in the laboratory model, including the output signal of the current regulator, in the transient state of the system

From the fragments of the output signal waveforms of the system current and current regulator, as shown in the inset to Fig. 15, the instant at which the TIC block activates the operation of the TIP block, and its effects, can be clearly seen.

The second stage of research on the laboratory model of the power supply focused on an evaluation of the static error in the voltage regulation on the DC link and its response time to a step change in the load value over a significant range, i.e. 10 times the load change. In this part of the study, the following waveforms were recorded: the currents, the reference signal for the current regulator, the DC voltage, and the output signal of the voltage regulator.

The range of working conditions of the laboratory model considered during these tests was similar to the operational conditions of the simulation model.

Exemplary waveforms of the currents and voltages in the tested system are shown in Fig. 16 (for rated voltage value in the DC link). This plot is functional equivalent of Fig. 10.

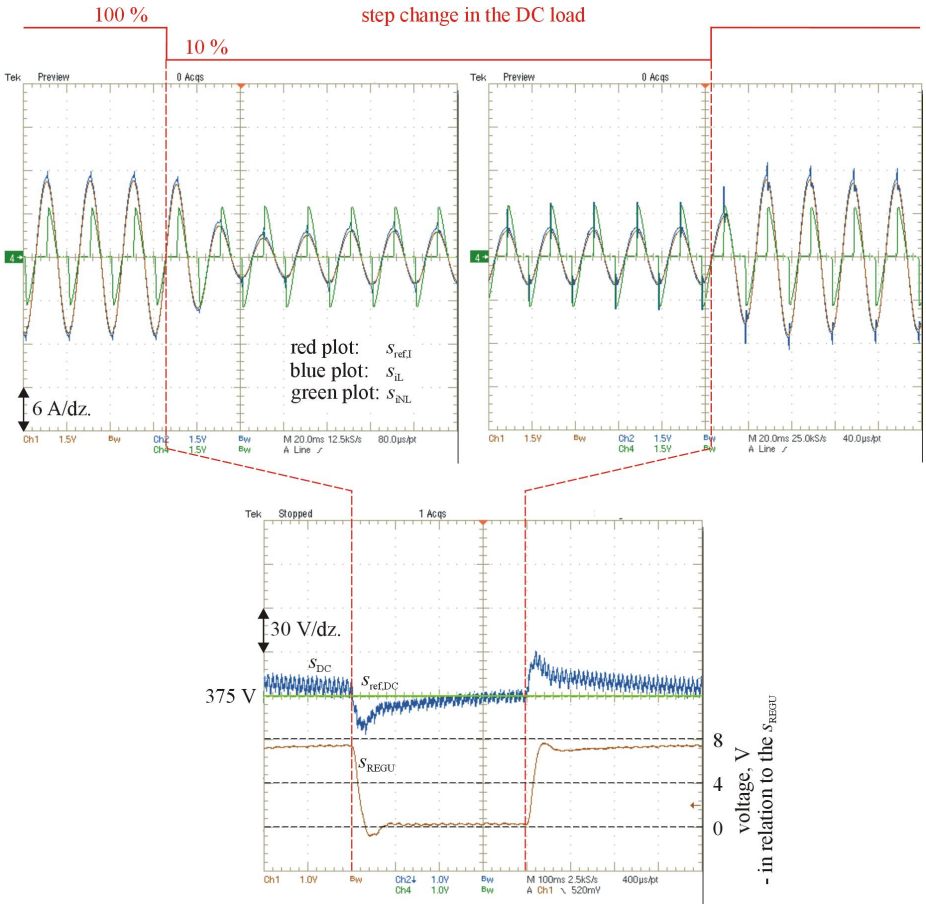

Fig. 16. Characteristic waveforms of signals in the laboratory model of the PSP, showing the system's response to a step change in the value of the DC load

Based on an analysis of the recorded waveforms, the value of the static adjustment error was estimated to be within a range of about ±1.5 V relative to the reference (setpoint) voltage. With respect to the rated voltage on the DC link, this means that the relative accuracy of regulation was within the range of 99.6% to 100.4% of the setpoint. The response time of the system to a step change in the value of the load on the DC link was in the range 50–75 ms (assuming that the voltage regulator's output signal reached 90% of its set value), corresponding to 2.5–3.5 periods of the line voltage. The range of response time resulted from such parameters as the value of the voltage on the DC bus, the percentage change in the load, the value of the line voltage, the time constants present in the control circuit, etc.

7. Conclusion

The results from the simulation and experimental models of the power supply compensator were largely consistent with each other. This was confirmed by the obtained waveforms and analyses of the values of the parameters *TWD* and τ_L for the system current under varying operating conditions of the entire system. The differences in the test results for the two models (to the disadvantage of the practical model) were mainly due to the difficulty of including in the simulation model all the operating parameters of the real model. In particular, this applied to the power line model, in which permanent transients occur under real conditions. The purpose of the proposed work has been achieved, i.e. as a result of the use of a tunable inductive filter, a marked reduction in the distortion of the line current was achieved in both models.

The authors expect the possibility of implementation in a commercial product. However, the solution is beneficial only when the developed power supply is used with non-linear loads with rapidly changing current.

References

[1] Rashid M.H., *Power Electronics Handbook*, Oxford: Elsevier Ltd., ISBN: 0-12-581650-2 (2018).

[2] Nazarko J., *State estimation of power distribution networks*, Scientific Dissertations No. 9 (in Polish), Bialystok University of Technology Publishing House, ISSN 0867-096X (1991).

[3] Akagi H., Watanabe E.H., Aredes M., *Instantaneous Power Theory and Applications to Power Conditioning*, John Wiley & Sons, Hoboken, NJ, USA, ISBN: 9781118362105 (2017).

[4] Ma Y., Hong F., Zhou X., Gao Z., *An overview on harmonic suppression*, 2018 Chinese Control and Decision Conference 412 (CCDC), Shenyang, China, pp. 4943–4948 (2018), DOI: 10.1109/CCDC.2018.8407987.

[5] Kurkowski M., Mirowski J., Popławski T., Pasko M., Białoń T., *Measurements of reactive energy in low voltage installations*, Przegląd Elektrotechniczny, vol. 1, no. 4, pp. 146–149 (2016).

[6] Hua-Wu L., Hong-Xing M., Jian-Feng J., Xi-Jun Y., Xing-Hua Y., *An EL-model based passivity control of four-phase interleaved PFC*, Archives of Electrical Engineering, vol. 62, no. 4, pp. 613–628 (2013), DOI: 10.2478/aee-2013-0049.

[7] Lu S. *et al.*, *A Family of Single-Stage AC/DC Converters Integrated Interleaved PFC and Resonant DC/DC Circuits*, IEEE Transactions on Power Electronics, vol. 38, no. 8, pp. 10026–10039 (2023), DOI: 10.1109/TPEL.2023.3278450.

[8] Fang J., Li X., Tang Y., *A review of passive power filters for voltage-source converters*, 2016 Asian Conference on Energy, Power and Transportation Electrification (ACEPT), pp. 1–6 (2016), DOI: 10.1109/ACEPT.2016.7811547.

[9] Klempka R., *Designing a group of single-branch filters taking into account their mutual influence*, Archives of Electrical Engineering, vol. 63, no. 1, pp. 81–91 (2014), DOI: 10.2478/aee-2014-0006.

[10] Pasko M., Buła D., Dębowski K., Grabowski D., Maciążek M., *Selected methods for improving operating conditions of three-phase systems working in the presence of current and voltage deformation – part II*, Archives of Electrical Engineering, vol. 67, no. 3, pp. 603–616 (2018), DOI: 10.24425/123666.

[11] Gwóźdź M., Wojciechowski R., *Possibility of using a tuned inductor in a power device to improve the quality of electricity*, Archives of Electrical Engineering, vol. 71, no. 4, pp. 1065–1080 (2022), DOI: 10.24425/aee.2022.142125.

[12] Szromba A., *Shunt power electronic buffer as active filter and energy flow controller*, Archives of Electrical Engineering, vol. 62, no. 1, pp. 55–75 (2013), DOI: 10.2478/aee-2013-0005.

[13] Maciążek M., Grabowski D., Pasko M., Lewandowski M., *Compensation based on active power filters – The cost minimization*, Applied Mathematics and Computation, vol. 267, pp. 648–654, ISSN 0096-3003 (2015), DOI: https://doi.org/10.1016/j.amc.2015.01.001.

[14] Pasko M., Buła D., *Hybrid active power filters*, Przegląd Elektrotechniczny (in Polish), vol. 83, no. 7/8, pp. 1–5 (2007).

[15] Ye T., Dai N., Zhu M., *Optimize the series LC design of a quasi proportional-resonant controlled hybrid active power filter for harmonic compensation*, Proceedings of the 2016 IEEE 11th Conference on Industrial Electronics and Applications (ICIEA), Hefei, China, pp. 624–629 (2016), DOI: https://doi.org/10.1109/ICIEA.2016.7603659.

[16] PN–EN 50160:2010 norm, *Parameters of supply voltage in public power grids*.

[17] Fryze S., *Active, reactive, and apparent power in circuits with nonsinusoidal voltage and current*, Przegląd Elektrotechniczny, vol. 13, pp. 193–203 (1931).

[18] Budeanu C., *Puissances reactives et fictives*, Impr. Cultura Națională, no. 2 (1927).

[19] Zajkowski K., *Disadvantages of the Budeanu and Fryze power theory in single-phase circuit*, Autobusy: Technika, Eksploatacja, Systemy Transportowe (in Polish), no. 12, pp. 1500–1504 (2016).

[20] Czarnecki L.S., *What is wrong with the conservative power theory (CPT)*, 2016 International Conference on Applied and Theoretical Electricity (ICATE), Craiova, Romania, pp. 1–6 (2016), DOI: 10.1109/ICATE.2016.7754619.

[21] Arranz-Gimon A., Zorita-Lamadrid A., Morinigo-Sotelo D., Duque-Perez O., *A review of total harmonic distortion factors for the measurement of harmonic and interharmonic pollution in modern power systems*, Energies, vol. 14, 6467 (2021), DOI: https://doi.org/10.3390/en14206467.

[22] Gwóźdź M., *Power electronics active shunt filter with controlled dynamics*, Proc. COMPEL: The International Journal for Computation and Mathematics in Electrical and Electronic Engineering, vol. 32, no. 4, pp. 1337–1344 (2013), DOI: https://doi.org/10.1108/03321641311317149.

[23] Zhang Z. *et al.*, *All-Fixed Switching Frequency Control of CRM Boost PFC Converter Based on Variable Inductor in a Wide Input Voltage Range*, 2019 IEEE Energy Conversion Congress and Exposition (ECCE), Baltimore, MD, USA, pp. 1434–1441 (2019), DOI: 10.1109/ECCE.2019.8913202.

[24] Zhang Z., Zhu F., Xu D., Krein P.T., Ma H., *An Integrated Inductive Power Transfer System Design With a Variable Inductor for Misalignment Tolerance and Battery Charging Applications*, IEEE Transactions on Power Electronics, vol. 35, no. 11, pp. 11544–11556 (2020), DOI: 10.1109/TPEL.2020.2987906.

[25] Wei Y., Luo Q., Du X., Altin N., Alonso J.M., Mantooth H.A., *Analysis and Design of the LLC Resonant Converter with Variable Inductor Control Based on Time-Domain Analysis*, IEEE Transactions on Industrial Electronics, vol. 67, no. 7, pp. 5432–5443 (2020), DOI: 10.1109/TIE.2019.2934085.

[26] Li Y. *et al*., *Extension of ZVS Region of Series–Series WPT Systems by an Auxiliary Variable Inductor for Improving Efficiency*, IEEE Transactions on Power Electronics, vol. 36, no. 7, pp. 7513–7525 (2021), DOI: 10.1109/TPEL.2020.3042011.

[27] Ciepliński Ł., Gwóźdź M., Wojciechowski R.M., *Application of a tuned inductor in a DC power supply with an active compensation function*, Energies, vol. 15, 6108 (2022), DOI: 10.3390/en15176108.

[28] Gwóźdź M., *The application of tuned inductors in electric power systems*, Energies, vol. 15, no. 22, 8481 (2022), DOI: org/10.3390/en15228481.

[29] Gwóźdź M., Wojciechowski R.M., Ciepliński Ł., *Power supply with parallel reactive and distortion power compensation and tunable inductive filter — Part 2*, Bulletin of the Polish Academy of Sciences Technical Sciences, vol. 69, no. 4, Article number: e137938 (2021), DOI: 10.24425/bpasts.2021.137938.

[30] Kaczorek T., Dzieliński A., Dąbrowski W., Łopatka R., *Fundamentals of control theory*, Publishing House WNT, Warszawa (in Polish) (2020).

[31] WWW Alfine-TIM, http://analog.alfine.pl/oferta/produkty-alfine, accessed 14.07.2023.